Published in final edited form as:
Traffic. 2012 May ; 13(5): 745–757. doi:10.1111/j.1600-0854.2012.01334.x.

Rabankyrin-5 interacts with EHD1 and Vps26 to regulate endocytic trafficking and retromer function

Jing Zhang[1], **Calliste Reiling**[1], **James B. Reinecke**[1], **Iztok Prislan**[2], **Luis A. Marky**[2], **Paul L. Sorgen**, **Naava Naslavsky**[1,*], and **Steve Caplan**[1,*]

[1]Department of Biochemistry and Molecular Biology and Eppley Cancer Center, University of Nebraska Medical Center, Omaha, Nebraska 68198-5870, USA

[2]Department of Pharmaceutical Sciences, University of Nebraska Medical Center, Omaha, Nebraska 68198-5870, USA

Abstract

Rabankyrin-5 (Rank-5) has been implicated as an effector of the small GTPase Rab5 and plays an important role in macropinocytosis. We have now identified Rank-5 as an interaction partner for the recycling regulatory protein EHD1. We have demonstrated this interaction by GST-pulldown, yeast two-hybrid assay, isothermal calorimetry, and co-immunoprecipitation and found that the binding occurs between the EH-domain of EHD1 and the NPFED motif of Rank-5. Similar to EHD1, we found that Rank-5 co-localizes and interacts with components of the retromer complex such as Vps26, suggesting a role for Rank-5 in retromer-based transport. Indeed, depletion of Rank-5 causes mislocalization of Vps26 and affects both the retrieval of mannose 6-phosphate receptor (M6PR) transport to the Golgi from endosomes and biosynthetic transport. Moreover, Rank-5 is required for normal retromer distribution, as over-expression of a wild-type Rank-5-siRNA-resistant construct rescues retromer mislocalization. Finally, we show that depletion of either Rank-5 or EHD1 impairs secretion of VSV-G. Overall, our data identify a new interaction between Rank-5 and EHD1, and novel endocytic regulatory roles that include retromer-based transport and secretion.

Keywords

retromer; Golgi; biosynthetic transport; secretion; VSV-G

INTRODUCTION

Endocytic trafficking is required for the transport and delivery of membranes and proteins. It is highly regulated by various proteins, including the C-terminal Eps15 homology domain (EHD) proteins. There are four mammalian family members, EHD1-4, and a single EHD ortholog in *C.elegans* (1) and *D. melanogaster* (2). EHD proteins are highly homologous and share 70–86% sequence identity, with EHD1 and EHD3 being the closest paralogs, and all EHD proteins have been implicated in regulating endocytic transport steps (3). Among them, EHD1 is the best-characterized, and has a well-established role in regulating recycling from the endocytic recycling compartment (ERC) to the plasma membrane [(4–7), and reviewed in (3)]. In addition, EHD1 can influence receptor internalization (8, 9), transport from pre-sorting endosomes to the ERC (10), and transport from early endosomes to the ERC (11).

*Address correspondence to: Steve Caplan scaplan@unmc.edu and Naava Naslavsky nnaslavsky@unmc.edu, Tel: 402-559-7556 FAX: 402-559-6650.

EHD1 and EHD3 also regulate retromer-mediated transport and affect Golgi morphology (12, 13), although the mechanism for this has remained enigmatic. The retromer controls retrograde transport from endosomes to the *trans*-Golgi network (TGN), and is critical for transport of the cation-independent mannose 6-phosphate receptor (CIMPR) and associated cargo molecules (14–16). The highly conserved mammalian retromer comprises two subcomplexes: a dimer of BAR domain-containing sorting nexin (SNX) 1, SNX 2, SNX 5, and SNX 6, and a heterotrimer composed of vacuolar protein sorting 26 (Vps26) A/B, Vps35, and Vps29 (17–23). The SNX subcomplex binds to phosphoinositides via Phox homology (PX) domains and induces membrane tubulation that is dependent on BAR domains (24–31). The Vps subcomplex is the cargo recognition complex (14), and its recruitment to membranes is catalyzed by Rab7 and inhibited by the Rab-GAP TBC1D5 (32, 33).

The diverse functions of EHD proteins are facilitated by multiple binding partners. EHD binding partners almost always contain the tripeptide asparagine-proline-phenyalanine (NPF), which is a motif that interacts with EHDs through the latter's EH-domain [reviewed in (3)]. Moreover, recent studies illustrate that an acidic cluster following the NPF motif is critical for EHD binding selectivity (34, 35). We recently identified a list of potential EHD binding proteins that contain an NPF motif followed by acidic residues (36). Among these candidate proteins, we took special interest in Rabankyrin-5 (ANFY1/Rank-5), whose only known function to date is that of a Rab5 effector involved in macropinocytosis (37). Rank-5 has an N-terminal BTB (Bric-a-brac, Tramtrack and Broad complex)/POZ (POx virus and Zinc finger) domain followed by 21 successive ankyrin repeats, and a C-terminal FYVE-finger domain (37–39) that binds to phosphatidylinositol-3-phosphate [PI(3)P]. Rank-5 localizes to early endosomes and macropinosomes, consistent in part with its described role in coordinating macropinocytosis (37).

In this study, we have identified Rank-5 as a novel binding partner of EHD1. Intriguingly, we found that Rank-5 co-localizes with and binds to the retromer Vps26 component and serves to regulate its subcellular localization. Our data support a new role for Rank-5 in the regulation of retromer-mediated transport and secretion from the Golgi, and provide a molecular basis for the function of EHD1 and Rank-5 in endosome-to-Golgi transport.

RESULTS

The Rank-5 NPFED motif mediates an interaction with EHD1

To test whether Rank-5 interacts with EHD1, we used GST-fused EH domains of EHD1-4 to pull-down Rank-5 from bovine brain cytosol. As shown in Figure 1A (upper panel), Rank-5 could be pulled down by GST fused to the EH domain of EHD1 (GST-EH1). On the other hand, GST-EH3 and GST-EH4 pulled-down barely detectable levels of Rank-5, and no pull-down was observed by either GST (Control) or GST-EH2. The amount of GST and GST-fusion proteins used in the pull-down assays is depicted by Coomassie blue staining (Figure 1A, lower panel). Using yeast two-hybrid analysis, binding of EH1 to Rank-5 was also detected (Figure 1B, 1st column, −His plate). Moreover, we confirmed the association of full-length (FL) EHD1 with wild-type (WT) Rank-5 (Figure 1B). Similar to the GST pull-down results, FL EHD3 exhibited weak binding to Rank-5, whereas no binding was observed for FL EHD2 and FL EHD4 (Figure 1B).

In previous studies, we and others have demonstrated that C-terminal EHDs selectively bind to proteins containing NPF motifs that are followed by acidic residues (34, 36). We therefore hypothesized that mutations in the Rank-5 NPFED motif might interfere with Rank-5-EHD1 interactions. As shown in Figure 1C, mutating the NPF motif to APA abolished the binding. Moreover, the binding was significantly decreased by mutating

NPFED to NPFAA. These findings indicate that both the NPF-motif and the flanking acidic residues are required for optimal Rank-5 binding to EHD1.

We further addressed the relevance of the acidic residues (following the NPF motif) by using Isothermal Titration Calorimetry (ITC) to measure binding affinities of WT Rank-5 NPFED and mutant NPFAA peptides with GST-EH1. We used a single site binding model to fit each calorimetric binding isotherm. The results of these fits and associated thermodynamic binding profiles are shown in Table 1. We obtained similar binding enthalpies of −3.6 kcal/mol (WT) and −4.0 kcal/mol (Mutant) and similar 1:1 stoichiometries (1 mol peptide per mol of protein). However, the K_b for binding of the wild type peptide was one order of magnitude higher than the K_b of the mutant peptide (Table 1), resulting in more favorable binding of wild type peptide to protein, by $\Delta\Delta G°_b = -1.3$ kcal/mol. Table 1 also shows that interaction of both ligands is accompanied with favorable $T\Delta S$ contributions. The binding of each peptide is both enthalpy and entropy driven. Favorable enthalpy contributions correspond to specific van der Waals interactions stabilizing complex formation, while the favorable entropic contributions includes water and ion releases overcoming the burial of the surfaces upon complex formation. The less favorable binding entropy of the mutant peptide is due to less favorable interacting entropy, perhaps because of its lower release of counterions and water molecules. These data indicate that the ED residues enhance Rank-5 binding affinity to EH1 significantly.

Rank-5 and EHD1 interact in cells

To determine if Rank-5 binds to EHD1 *in vivo*, we performed co-immunoprecipitation analysis. Cells were transfected with either GFP-Rank-5 or GFP vector alone as a control (Figure 2A–C). Protein expression levels were assessed by immunoblot analysis (Figure 2A), and the effectiveness of immunoprecipitations was demonstrated (Figure 2B). As shown in Figure 2C, GFP-Rank-5 immunoprecipitated endogenous EHD1 from the total lysate, whereas the GFP control did not.

Rank-5 has also been observed in association with vesicular structures (37). To determine whether EHD1 and Rank-5 colocalize, we used specific antibodies that recognize the endogenous proteins (Figure 2, D–F). Rank-5 partially colocalized with EHD1 on vesicular structures. These data indicate that Rank-5 and EHD1 might functionally interact in endocytic pathways.

EHD1 plays a role upstream of Rank-5

We next asked what impact depletion of one binding partner has on the localization of the other. To address this, we utilized a siRNA approach to impede expression of either Rank-5 or EHD1 in HeLa cells. As depicted, expression of either endogenous Rank-5 (Figure 3A) or endogenous EHD1 (Figure 3B) was reduced by ~ 90% upon siRNA treatment. To examine the effect of Rank-5 depletion on EHD1 localization, HeLa cells were transfected with GFP-Myc-EHD1 (because antibodies to the endogenous protein elicit a relatively weak staining pattern). No change in the localization of EHD1 was observed upon Rank-5-depletion (Figure 3, C and D). On the contrary, EHD1-depletion caused a considerably altered subcellular localization of endogenous Rank-5 from the cell periphery (in Mock-treated cells; Figure 3E) to the perinuclear area in cells lacking EHD1 (Figure 3F). These data indicate that EHD1 controls Rank-5 localization and likely functions upstream of Rank-5.

Rank-5 co-localizes with the retromer subunit Vps26

Since both EHD1 and EHD3 have been physically and/or functionally linked to the retromer complex (12, 13), we hypothesized that Rank-5 might also associate with the retromer. To determine whether Rank-5 colocalizes with the retromer, HeLa cells were stained with

specific antibodies that recognize endogenous Rank-5 and the retromer subunit Vps26 protein. As indicated in Figure 4A–C, Rank-5 and Vps26 displayed partial co-localization on vesicular structures (see arrows). To determine whether Rank-5 forms a complex with the retromer, co-immunoprecipitation was performed. HeLa cells were transfected with GFP-Rank-5 or GFP vector as control, and expression of the proteins was assessed by immunoblot (Figure 4D). As shown in Figure 4E, GFP-Rank-5 immunoprecipitated endogenous Vps35 and Vps26 from the lysate, but not SNX2. MICAL-L1, an EHD1 binding partner, was also detected in the immunoprecipitates. These data indicate that Rank-5 associates with the cargo recognition subcomplex of the retromer, suggesting a potential role for Rank-5 in the regulation of endosome-to-Golgi transport.

Since the localization of both Rank-5 and the retromer complex subunits are affected by EHD1-depletion, we next analyzed whether Rank-5 co-localization with Vps26 is impacted by EHD1 knock-down. Compared to Mock-treated cells (Figure 4A–C and F–H), depletion of EHD1 led to a 23% increase in the co-localization of Rank-5 and Vps26, mostly in the perinuclear region (Figure 4, I–K; quantified in L).

To characterize the perinuclear region to which Rank-5 localizes upon EHD1-depletion, we performed immunostaining with a series of markers (Figure S1). As shown, upon EHD1 knock-down, Rank-5 displayed only very partial overlap with either Giantin (Figure S1, A–F) or GFP-Rab11 (Figure S1, G–L). Similarly, Vps26 displayed little overlap with GFP-Rab11 upon EHD1-siRNA treatment (Figure S1, M–R). These results indicate that Rank-5 and Vps26 accumulate in a Golgi proximal region, but display only minor overlap with the Golgi or ERC upon EHD1-depletion.

Since EHD1 is involved in the regulation of endocytic recycling, we asked whether Rank-5 knock-down might affect the recycling of cargo such as the transferrin receptor (TfR) and major histocompatibility class I (MHC-I) molecules. HeLa cells were Mock-treated or treated with Rank-5-siRNA, and assayed for transferrin (Tf) uptake. In Mock-treated cells, after 5 min of uptake the internalized Tf was still primarily localized to peripheral endosomes (Figure S2A). On the other hand, in Rank-5-depleted cells, Tf was rapidly internalized and accumulated in the perinuclear area (Figure S2B). The amount of Tf internalized measured by flow cytometry displayed a 49% increase in cells depleted of Rank-5 (Figure S2C). To investigate the effect of Rank-5 depletion on recycling, Mock or siRNA-treated cells were pulsed with Tf for 5 min and then incubated with complete medium (“chased”) for the indicated time points. As demonstrated, the recycling of Tf was only modestly delayed in Rank-5 depleted cells (about 14%, Figure S2, D–I).

Similarly, we performed MHC-I uptake and recycling assays in Mock- and Rank-5-siRNA treated cells. Uptake of MHC-I was accelerated by about 32% in Rank-5 depleted cells (Figure S3, A–C), and a minor delay in recycling was also observed (Figure S3, D–I). These data suggest that Rank-5 is involved in clathrin-dependent and -independent internalization pathways in addition to its role in macropinocytosis (37).

EHD1 and Rank-5 associate with the retromer independently of each other

EHD1 interacts with the retromer and co-immunoprecipitates with Vps26 (12), but whether this interaction is direct remains unknown. To investigate whether Rank-5 is required for this interaction, we knocked it down by siRNA (Figure 5A) and then performed co-immunoprecipitations between EHD1 and Vps26. As shown in Figure 5B, EHD1 remained associated with Vps26 even upon depletion of Rank-5.

To determine whether EHD1 and Vps26 remain in close proximity in the absence of Rank-5, HeLa cells were either Mock- or Rank-5-siRNA-treated, and GFP-Myc-EHD1 was

expressed in these cells. Cells were then incubated with anti-Myc and anti-Vps26 antibodies and subjected to a Duolink proximity assay. Protein pairs within ~ 40 nm of each other are depicted by white dots. EHD1 and MICAL-L1 were used as a positive control (40) (Figure 5, C and D; see white dots), while the GFP vector co-transfected with Vps26 was used as a negative control and displayed no reaction dots (Figure 5, E and F). As indicated, the close proximity between EHD1 and Vps26 remained even upon Rank-5-depletion (Figure 5, G–J). These data suggest that although Rank-5 associates with both EHD1 and Vps26, EHD1 interacts with Vps26 in a Rank-5-independent manner. Similarly, EHD1 depletion by siRNA treatment (Figure 5K) had little effect on the association between Rank-5 and Vps26 (Figure 5L), suggesting that Rank-5 interacts with Vps26 independently of EHD1.

Depletion of Rank-5 affects localization of Vps26

Given the association of Rank-5 with the retromer, we next asked whether Rank-5 influences the subcellular localization of the retromer complex. In Mock-treated cells, the retromer complex subunit Vps26 localized primarily to peripheral endosomes, with a pool of Vps26 co-localized with GM130 (Figure 6, A–C; quantified in G). Upon Rank-5-siRNA treatment, Vps26 redistributed to the perinuclear region and demonstrated a 31% increased level of co-localization with GM130 (Figure 6, D–F; quantified in G). Similarly, Rank-5 depletion relocalized SNX2 to the Golgi region, possibly through an indirect mechanism (data not shown). Rank-5 depletion did induce relocalization of a significant portion of Rab5-containing endosomes to the perinuclear area (Figure S4). Nevertheless, many Rab5-containing endosomes were still largely peripheral. Thus while Rank-5 depletion did effect endosome positioning, its absence affected Vps26-containing vesicles even more dramatically. Therefore, both endosomal repositioning and potential lack of Vps26-containing vesicle fusion with the Golgi might account for the observed phenotypes.

To determine whether re-introduction of Rank-5 could rescue the altered Vps26 localization in Rank-5-depleted cells, we first transfected a siRNA-resistant form of the protein and examined the effectiveness of its expression by immunoblot. HeLa cells transfected with WT GFP-Rank-5 exhibited >90% knock-down of both endogenous Rank-5 and GFP-Rank-5 proteins in siRNA-treated cells (Figure 6H, lane 2) compared to Mock (Figure 6H, lane 1). However, when Rank-5-depleted cells were transfected with the siRNA-resistant-GFP-Rank-5, both endogenous Rank-5 and GFP-Rank-5 protein levels remained similar to Mock-treated cells (compare Figure 6H, lanes 3 and 4).

We next transfected the WT siRNA-resistant GFP-Rank-5 into siRNA-treated cells and examined the localization of Vps26. As shown in Figure 6I–L, transfected cells displayed a normal pattern of relatively dispersed Vps26 (see cells in yellow border) as opposed to the Golgi-centralized pattern observed in non-transfected cells lacking Rank-5. 60% rescue in WT siRNA-resistant Rank-5 transfected cells (Resist-Rank-5) was observed (Figure 6Q). On the other hand, introduction of a siRNA-resistant Rank-5 mutant lacking a functional NPF motif (Resist-Rank-5-APA) was unable to rescue the peri-Golgi clustering of Vps26 in cells lacking Rank-5 (Figure 6, M–P, quantified in Q). These data indicate that Rank-5 and its binding to EHD1 are required for controlling the localization of Vps26.

Rank-5 depletion affects both the retrieval of M6PR from endosomes to the Golgi and cathepsin D transport

The retromer complex is required for endosome-to-Golgi transport (14, 16, 31), and an impaired endosome-to-Golgi axis can lead to delayed biosynthetic transport to late endosomes and lysosomes (13, 14, 16). We therefore analyzed the effect of Rank-5 knock-down on endosome-to-Golgi retrieval. HeLa cells grown on cover-slips were treated with Rank-5-siRNA and subjected to a M6PR antibody uptake assay. We observed a 17%

reduction of M6PR at the Golgi in siRNA-treated cells after 30 min of antibody uptake. In WT siRNA-resistant Rank-5 transfected cells, approximately 60% rescue of M6PR transport to the Golgi was observed (Figure 7A). Similarly, EHD1- (Figure S5A) or Vps26- (Figure S5B) depletion reduced the M6PR transport to the Golgi. Consistent with these findings, there is a significant increase in the subcellular localization of cathepsin D, a lysosomal lumenal hydrolase, at the Golgi region upon Rank-5-siRNA treatment (Figure 7, C–H, quantified in B). There is a minor, yet significant corresponding decrease of cathepsin D in lysosomes upon Rank-5 depletion (Figure S6, A–G).

The AP-1 adaptor complex was also examined because of its involvement in Golgi-to-endosome transport (41). When Rank-5 was depleted from cells, there was an increase in γ-adaptin localized to the Golgi area (Figure S7, A–G). However, Rank-5 knock-down had no obvious effect on Arf1, an important factor in the recruitment of AP-1 to the Golgi (Figure S7, H–N). Overall, these results demonstrate that Rank-5 plays a role in the endosome-to-Golgi retrieval and biosynthetic transport from the Golgi.

Rank-5 and EHD1 are required for efficient VSV-G secretion

Since the Golgi is critical for secretion as well as biosynthetic transport, we assessed whether EHD1 and Rank-5 affect secretion. HeLa cells were either Mock-treated or treated with either Rank-5-siRNA or EHD1-siRNA. They were then transfected with a temperature-sensitive mutant of GFP-VSV-G. The cells were incubated at 40°C for 18 h to allow the accumulation of newly synthesized GFP-VSV-G in the ER. Secretion of VSV-G was then performed by shifting the cells to 32°C for various time points. As shown in Figure 7I, secretion of VSV-G was significantly decreased at all time points upon EHD1-knock-down. Knock-down of Rank-5 also impaired VSV-G secretion at 2 h and 3 h, to a lesser extent than EHD1-knock-down. Vps26-depletion had little or no effect on VSV-G secretion (data not shown). These results suggest that EHD1 and Rank-5 are involved in the secretion of VSV-G, possibly through their effects on normal maintenance of membrane flow to the Golgi.

DISCUSSION

Recent studies have demonstrated that the selectivity of the C-terminal EH-domain for NPF motifs is greatly enhanced when the phenylalanine is followed by at least two acidic residues (34, 36). After searching the databank for proteins containing the motif N-P-F-[D/E]-[D/E] (36), we chose Rank-5 (N-P-F-E-D) for further investigation because it is a Rab5 effector with a known function in endocytosis/macropinocytosis (37).

We have identified Rank-5 as a novel binding partner of EHD1 *in vitro* (Figure 1 and Table 1) and *in vivo* (Figure 2). Moreover, we confirmed that the NPF tripeptide and the subsequent acidic residues are necessary for optimal binding (Figure 1C and Table 1). Three other Rab effectors, all containing NPF motifs followed by acidic clusters, have been reported as EHD-binding proteins: 1) Rabenosyn-5, a divalent Rab4/Rab5 effector that binds to EHD1 through the first two of its five NPF motifs (42); 2) Rab11-FIP2, the only known Rab11 effector that contains three NPF motifs (43), binds to both EHD1 and EHD3 (44); and 3) MICAL-L1, a Rab8a and Rab35 interaction partner that binds EHD1 and recruits it to tubular membranes (40, 45). These proteins serve as common interaction partners for both Rab and EHD families, potentially coordinating endocytic transport events (3, 46).

Whereas EHD1 regulates the recycling of cargos from ERC to the plasma membrane [(4–7), and reviewed in (3)], Rank-5 is known to modulate macropinocytosis (37). However, since Rank-5 partially co-localized with endosomes, we posited that its binding to EHD1 might impact endocytic recycling. Surprisingly, knockdown of Rank-5 only moderately delayed the recycling of Tf and MHC-I, whereas a significant increase in uptake of both Tf and

MHC-I was observed (Figure S2 and S3). In EGF-stimulated A431 cells, transferrin uptake was not significantly altered upon Rank-5-depletion (37), suggesting that under conditions in which macropinocytosis is not activated, Rank-5 may carry out additional trafficking steps.

Since Rank-5 had only a marginal effect on recycling, we searched for other potential functions that might be mediated by Rank-5 binding to EHD1. EHD1 and EHD3 regulate the retromer complex and endosome-to-Golgi retrograde transport (12, 13). Our data indicate that Rank-5 interacts with the retromer complex Vps26 subunit and Vps35 (Figure 4) and regulates subcellular localization of the complex (Figure 6). EHD1 itself interacts with the retromer and stabilizes SNX1 tubules (12), and the recruitment of the Vps complex requires the the GTP binding proteins Rab5 and Rab7 (32, 33). It is likely that through its interactions with both EHD1 and Rab5 that Rank-5 affects the regulation of retromer localization.

Although EHD1 interacts with the retromer *in vivo*, it is unclear whether this is by a direct interaction (12). Our yeast-two hybrid results suggest that there is no direct binding between either EHD1 and Vps26 or Rank-5 and Vps26 (data not shown). Co-immunoprecipitation between EHD1 and Vps26 indicates that EHD1 interacts with the retromer complex independently of Rank-5, since knockdown of the latter has no effect on EHD1-retromer interactions (Figure 5). Similarly, EHD1 is not required for Rank-5 association with Vps26 (Figure 5). The SNX dimer and Rank-5 bind to PI(3)P-enriched endosomal membranes via their PX domain (25, 26, 31) and FYVE domain (37), respectively. Our data lead us to suggest that both EHD1 and Rank-5 indirectly associate with retromer complex subunits, and the precise mode of this binding will necessitate further study.

The retromer complex is required for endosome-to-TGN transport (14, 16, 31, 47), and impaired retromer function can lead to delayed biosynthetic transport of lysosomal hydrolases from the Golgi (13, 14, 16). The functional consequence of Rank-5-depletion on the retromer was a significant reduction of M6PR retrieval from endosomes and retention of cathepsin D in the Golgi region (Figure 7). Moreover, Rank-5-depletion led to increased co-localization of γ-adaptin with the Golgi (Figure S7). This is consistent with the finding that in EHD3-depleted cells, retrieval of CI-M6PR and recruitment of γ-adaptin are compromised, leading to impaired transport of cathepsin D from the Golgi (13).

In addition to its effects on endosome-to-Golgi retrieval and biosynthetic transport, both Rank-5- and EHD1-depletion delayed secretion from the Golgi as determined utilizing a temperature-sensitive VSV-G mutant (Figure 7I), whereas knock-down of Vps26 had little effect on VSV-G secretion (data not shown). Indeed, the retromer is also involved in the retrieval of Wntless to promote the secretion of Wnt proteins (48–53). One potential explanation for the effects of Rank-5 and EHD1 on secretion is that their depletion impacts retromer function and thus indirectly affects the maintenance of Golgi membranes and morphology (13), compromising VSV-G secretion. The delay in VSV-G secretion upon EHD1 depletion might also be related to the effect of EHD1 on recycling endosomes (54). Further investigation will be needed to understand the underlying mechanisms.

Overall, we have identified Rank-5 as a novel binding partner of EHD1, both *in vitro* and *in vivo*, and have discerned a new role for Rank-5 in regulating retromer-mediated transport in an EHD1-dependent manner.

MATERIALS AND METHODS

Recombinant DNA Constructs

Cloning of the glutathione S-transferase (GST)-EH domains of EHD1-4, and GFP-Myc-EHD1 have been described previously (4, 40, 42). Human Rabankyrin-5 (Rank-5) was obtained by PCR from a brain cDNA library (Clontech, Mountain View, CA) and cloned into TOPO XL vector (Invitrogen, Carlsbad, CA). Rank-5 was subcloned into EGFP-C3 vector and pGADT7 two-hybrid vectors. NPF mutants and siRNA-resistant constructs were generated using the QuikChange site-directed mutagenesis kit (Stratagene, La Jolla, CA). Temperature-sensitive GFP-vesicular stomatitis virus glycoprotein (GFP-VSV-G) was kindly provided by Dr. J. Donaldson (NIH, MD).

Antibodies and Reagents

Affinity-purified rabbit polyclonal antibodies directed against human EHD1 were described previously (42). Mouse anti-Rank-5 was from Abnova (Taipei City, Taiwan); mouse anti-actin was from Novus Biologicals (Littleton, CO); mouse anti-SNX2 and mouse anti-GM130 were from BD Transduction Labs (Franklin Lakes, NJ); sheep anti-TGN46 was from Serotec (Raleigh, NC); mouse anti-GFP was from Roche Applied Science (Indianapolis, IN); mouse anti-Cathepsin D was from Santa Cruz (Santa Cruz, CA); rabbit anti-Giantin, rabbit anti-Vps26 and rabbit anti-Vps35 were from Abcam (Cambridge, MA); W6/32 antibody to MHC-I (peptide-bound) was obtained from the American Type Culture Collection (Manassas, VA); mouse anti-M6PR was from BioLegend (San Diego, CA); mouse anti-VSV-G (clone 8G5FL11) was from KeraFAST (Winston-Salem, NC); Goat anti-mouse horseradish peroxidase (HRP) and donkey anti-rabbit HRP were obtained from Jackson ImmunoResearch Laboratories (West Grove, PA); Secondary Cy5-conjugated anti-mouse, Alexa Fluor 488 or 568 anti-mouse and anti-rabbit were from Molecular Probes (Eugene, OR).

GST Pulldown and Co-Immunoprecipitation

GST pull-downs were performed as described previously (42). Briefly, purified GST-EH1, GST-EH2, GST-EH3, GST-EH4 fusion proteins were incubated with glutathione-Sepharose beads in phosphate-buffered saline (PBS) with 1% Triton X-100 and 0.25mM 4-(2-aminoethyl)-benzenesulfonyl fluoride hydrochloride (AEBSF) for 2 h at 4°C. Beads were washed four times and incubated with bovine brain cytosol (BBC) at 4°C overnight. Beads were sedimented and new BBC added and incubated for 4 h. This step was repeated, beads were washed, and the eluted proteins were separated by SDS-PAGE and immunoblotted with appropriate antibodies.

For co-immunoprecipitation, transfected cells were lysed in buffer containing 50 mM Tris, pH 7.4, 150 mM NaCl, 0.5% TX-100, 1.8 mg/ml iodoacetamide and protease inhibitors cocktail (Calbiochem, Gibbstown, NJ). Protein L-Sepharose beads (Thermo Fisher Scientific, Rockford, IL) were incubated with anti-GFP antibody for 2 h at 4°C, followed by three washes with PBS. Lysates were immunoprecipitated with the antibody-bound beads overnight at 4°C. Immunoprecipitates were washed, eluted, and resolved by SDS-PAGE.

Yeast Two-Hybrid Analysis

The yeast two-hybrid assay was described previously (44). Briefly, Gal4AD and Gal4BD constructs were co-transformed into the *Saccharomyces cerevisiae* strain AH109 by the lithium acetate procedure as described in the instructions for the MATCHMAKER two-hybrid kit (BD Biosciences Clontech, Palo Alto, CA). The co-transformants were streaked on plates lacking leucine and tryptophan and incubated at 30°C for 3 days. An average of four colonies were then chosen and suspended in water. Optical density was measured at

600 nm and an equal amount of yeast was spotted on plates lacking leucine and tryptophan (+HIS) as well as plates also lacking histidine (−HIS). Plates were then incubated at 30°C until growth of the colonies.

Isothermal Titration Calorimetry (ITC)

Rank-5 wildtype NPF-motif peptide ITVSSDQSVNPFEDVPVV and mutant peptide ITVSSDQSVNPFAAVPVV were synthesized by GenScript (Piscataway, NJ). The heat for the reaction of each peptide with the protein was measured directly by isothermal titration calorimetry using the iTC_{200} titration calorimeter from Microcal (Northampton, MA). ITC binding isotherms were obtained as follows; 21 injections of 0.7–2.2 μL peptide (1.2 mM) were used to titrate a 250 μL protein solution (75 μM) in the reaction cell at 25 °C, the effective volume of this cell is 200 μL. The reaction heat of each injection is measured by integration of the area of the injection peak, corrected for the dilution heat of the peptide, and normalized by the moles of peptide added. The resulting calorimetric binding isotherm, Heat/(mole of injectant) vs. [peptide]/[protein], were fitted with the Origin 7 software, supplied by Microcal, Inc. We used a model of one single binding site to fit each binding isotherms. These fits are characterized by a set of three parameters: binding constant (K_b), binding enthalpy (ΔH_b) and number of sites (n). The Gibbs free energy, $\Delta G°_b$ were determined from the equation: $\Delta G_b° = -RT\ln K_b$, where R is the molar gas constant and T is a temperature at which experiment is performed. The entropy of binding, ΔS_b, was calculated from the Gibbs equation.

Gene Knockdown by siRNA and Rescue using siRNA-Resistant Rank-5 Expression

Oligonucleotide duplexes targeting human Rank-5 or EHD1 (Dharmacon, Lafeyette, CO) were transfected using oligofectamine (Invitrogen) for 48 h as previously described (42). The siRNA-resistant rescue construct of Rank-5 was transfected using FuGENE HD (Roche Applied Science).

Immunofluorescence, Uptake and Recycling Assays, and Quantification

Immunofluorescence staining of HeLa cells was performed as described previously (42, 55). Images were acquired on an LSM 5 Pascal confocal microscope (Carl Zeiss, Thornwood, NY) by using a 63X 1.4 numerical aperture objective with appropriate filters. Transferrin and MHC-I uptake and recycling assays were done as described previously (42). Quantification of colocalization was done using ImageJ.

Duolink Assay

Duolink kit was purchased from Olink Bioscience (Uppsala, Sweden), and the assay was done according to the manufacturer's protocol. Briefly, HeLa cells grown on coverslips were treated with or without Rank-5-siRNA, and transiently transfected with GFP-Myc-EHD1. The coverslips were then incubated with primary antibodies that bind to the proteins to be detected: mouse anti-Myc for EHD1 and rabbit anti-Vps26 antibodies. After 1 h of incubation, the cells were washed in PBS and secondary antibodies conjugated with PLA probe MINUS and PLUS were added to the reaction and incubated for 1 h at 37°C. The cells were washed and a ligation solution consisting of two oligonucleotides and the ligase was added. If the antibodies are in close proximity (< 40 nm), the oligonucleotides will hybridize to the two PLA probes and join to form a closed circle. The amplification solution consisting of fluorescently labeled oligonucleotides and polymerase was added, which allows the signal to be amplified and visualized as a distinct fluorescent spot to be analyzed by fluorescence microscopy.

Anti-M6PR Uptake Assay

HeLa cells were grown on coverslips and treated with or without Rank-5-siRNA. The coverslips were then washed with PBS, and incubated with anti-M6PR antibody for 30 min at 37°C in complete medium. Cells were washed and fixed in 4% paraformaldehyde followed by Golgi staining and the subsequent secondary antibody staining. Quantification of M6PR at the Golgi was done using LSM Pascal software.

Quantitative Measurements of Uptake by Flow Cytometry

Cells were serum starved in DMEM containing 0.5% bovine serum albumin for 30 min, and then incubated with Tf-633 (Invitrogen) for a 5 min pulse at 37°C. Cells were washed with PBS, trypsinized, and transferred to pre-cooled tubes containing 10 ml of ice-cold DMEM, and pelleted by centrifugation. Cell pellets were fixed in 300 μl of 4% paraformaldehyde. At least 10,000 cells were analyzed for internalized Tf-633 by flow cytometry analysis (BD Biosciences, San Jose, CA). For MHC-I uptake, cells were gently dislodged by CellStripper (Mediatech Inc., Manassas, VA) and washed three times with PBS. Cells were gently rotated in the presence of W6/32 anti-MHC-I for 1 h, followed by a 20 s acid strip (0.5% acetic acid, 500 mM NaCl) to remove residual surface-bound antibody (42). Cells were then washed, fixed, incubated with secondary Cy5-conjugated anti-mouse antibody, and analyzed by flow cytometry.

VSV-G Trafficking

HeLa cells were grown on coverslips or 35 mm dishes and treated with siRNA for 48 h. A temperature-sensitive mutant of GFP-VSV-G (56) was transfected in parallel with siRNA. During the last 18 h, cells were transferred to 40°C to allow accumulation of newly synthesized GFP-VSV-G in the ER. To measure VSV-G trafficking, cells were pre-incubated with complete medium supplemented with 20 mM HEPES and 100 μg/ml cycloheximide (57) for 30 min, and shifted to 32°C for various time points. GFP-VSV-G reaching the plasma membrane was either visualized by confocal microscopy or measured by flow cytometry by binding to a mouse anti-VSV-G antibody followed by a secondary Cy5-conjugated anti-mouse antibody. Secreted VSV-G was calculated at each time point by dividing surface-expressed VSV-G (Cy5) by overall GFP-VSV-G expressed (GFP), and subtracting the baseline values at 0 h. Values were normalized in reference to the Mock 3 h value denoted as 100.

Supplementary Material

Refer to Web version on PubMed Central for supplementary material.

Acknowledgments

The authors gratefully acknowledge the support of National Institutes of Health grants R01GM074876 (SC and NN), and R01GM087455 (SC), the Nebraska Dept. of Health (NN), and P20 RR018759 from the National Center for Research Resources (SC and NN). This work was also supported by Grant MCB-0616005 from the National Science Foundation, and a Shared Instrumentation Grant 1S10RR027205 from the National Institutes of Health (LAM). Partial financial support (to I.P.) from the Slovenian Research Agency (P1 0201) is greatly appreciated.

References

1. Grant B, Zhang Y, Paupard MC, Lin SX, Hall DH, Hirsh D. Evidence that RME-1, a conserved C. elegans EH-domain protein, functions in endocytic recycling. Nat Cell Biol. 2001; 3(6):573–579. [PubMed: 11389442]

2. Olswang-Kutz Y, Gertel Y, Benjamin S, Sela O, Pekar O, Arama E, Steller H, Horowitz M, Segal D. Drosophila Past1 is involved in endocytosis and is required for germline development and survival of the adult fly. Journal of Cell Science. 2009; 122(Pt 4):471–480. [PubMed: 19174465]

3. Naslavsky N, Caplan S. EHD proteins: key conductors of endocytic transport. Trends in Cell Biology. 2011; 21(2):122–131. [PubMed: 21067929]

4. Caplan S, Naslavsky N, Hartnell LM, Lodge R, Polishchuk RS, Donaldson JG, Bonifacino JS. A tubular EHD1-containing compartment involved in the recycling of major histocompatibility complex class I molecules to the plasma membrane. EMBO J. 2002; 21(11):2557–2567. [PubMed: 12032069]

5. Guilherme A, Soriano NA, Furcinitti PS, Czech MP. Role of EHD1 and EHBP1 in perinuclear sorting and insulin-regulated GLUT4 recycling in 3T3-L1 adipocytes. Journal of Biological Chemistry. 2004; 279(38):40062–40075. [PubMed: 15247266]

6. Jovic M, Naslavsky N, Rapaport D, Horowitz M, Caplan S. EHD1 regulates beta1 integrin endosomal transport: effects on focal adhesions, cell spreading and migration. Journal of Cell Science. 2007; 120(Pt 5):802–814. [PubMed: 17284518]

7. Lin SX, Grant B, Hirsh D, Maxfield FR. Rme-1 regulates the distribution and function of the endocytic recycling compartment in mammalian cells. Nat Cell Biol. 2001; 3(6):567–572. [PubMed: 11389441]

8. Naslavsky N, Rahajeng J, Rapaport D, Horowitz M, Caplan S. EHD1 regulates cholesterol homeostasis and lipid droplet storage. Biochemical and Biophysical Research Communications. 2007; 357(3):792–799. [PubMed: 17451652]

9. Yap CC, Lasiecka ZM, Caplan S, Winckler B. Alterations of EHD1/EHD4 protein levels interfere with L1/NgCAM endocytosis in neurons and disrupt axonal targeting. Journal of Neuroscience. 2010; 30(19):6646–6657. [PubMed: 20463227]

10. Cai B, Katafiasz D, Horejsi V, Naslavsky N. Pre-sorting endosomal transport of the GPI-anchored protein, CD59, is regulated by EHD1. Traffic. 2010; 12(1):102–120. [PubMed: 20961375]

11. Rahajeng J, Giridharan SS, Naslavsky N, Caplan S. Collapsin response mediator protein-2 (Crmp2) regulates trafficking by linking endocytic regulatory proteins to dynein motors. Journal of Biological Chemistry. 2010; 285(42):31918–31922. [PubMed: 20801876]

12. Gokool S, Tattersall D, Seaman MN. EHD1 interacts with retromer to stabilize SNX1 tubules and facilitate endosome-to-Golgi retrieval. Traffic. 2007; 8(12):1873–1886. [PubMed: 17868075]

13. Naslavsky N, McKenzie J, Altan-Bonnet N, Sheff D, Caplan S. EHD3 regulates early-endosome-to-Golgi transport and preserves Golgi morphology. Journal of Cell Science. 2009; 122(Pt 3):389–400. [PubMed: 19139087]

14. Arighi CN, Hartnell LM, Aguilar RC, Haft CR, Bonifacino JS. Role of the mammalian retromer in sorting of the cation-independent mannose 6-phosphate receptor. Journal of Cell Biology. 2004; 165(1):123–133. [PubMed: 15078903]

15. McGough IJ, Cullen PJ. Recent advances in retromer biology. Traffic. 2011; 12(8):963–971. [PubMed: 21463457]

16. Seaman MN. Cargo-selective endosomal sorting for retrieval to the Golgi requires retromer. Journal of Cell Biology. 2004; 165(1):111–122. [PubMed: 15078902]

17. Bonifacino JS, Hurley JH. Retromer. Current Opinion in Cell Biology. 2008; 20(4):427–436. [PubMed: 18472259]

18. Bonifacino JS, Rojas R. Retrograde transport from endosomes to the trans-Golgi network. Nat Rev Mol Cell Biol. 2006; 7(8):568–579. [PubMed: 16936697]

19. Bugarcic A, Zhe Y, Kerr MC, Griffin J, Collins BM, Teasdale RD. Vps26A and Vps26B subunits define distinct retromer complexes. Traffic. 2011; 12(12):1759–1773. [PubMed: 21920005]

20. Haft CR, de la Luz Sierra M, Bafford R, Lesniak MA, Barr VA, Taylor SI. Human orthologs of yeast vacuolar protein sorting proteins Vps26, 29, and 35: assembly into multimeric complexes. Molecular Biology of the Cell. 2000; 11(12):4105–4116. [PubMed: 11102511]

21. Hierro A, Rojas AL, Rojas R, Murthy N, Effantin G, Kajava AV, Steven AC, Bonifacino JS, Hurley JH. Functional architecture of the retromer cargo-recognition complex. Nature. 2007; 449(7165):1063–1067. [PubMed: 17891154]

22. Kerr MC, Bennetts JS, Simpson F, Thomas EC, Flegg C, Gleeson PA, Wicking C, Teasdale RD. A novel mammalian retromer component, Vps26B. Traffic. 2005; 6(11):991–1001. [PubMed: 16190980]
23. Koumandou VL, Klute MJ, Herman EK, Nunez-Miguel R, Dacks JB, Field MC. Evolutionary reconstruction of the retromer complex and its function in Trypanosoma brucei. Journal of Cell Science. 2010; 124(Pt 9):1496–1509. [PubMed: 21502137]
24. Carlton JG, Bujny MV, Peter BJ, Oorschot VM, Rutherford A, Arkell RS, Klumperman J, McMahon HT, Cullen PJ. Sorting nexin-2 is associated with tubular elements of the early endosome, but is not essential for retromer-mediated endosome-to-TGN transport. Journal of Cell Science. 2005; 118(Pt 19):4527–4539. [PubMed: 16179610]
25. Cullen PJ, Cozier GE, Banting G, Mellor H. Modular phosphoinositide-binding domains--their role in signalling and membrane trafficking. Current Biology. 2001; 11(21):R882–893. [PubMed: 11696348]
26. Merino-Trigo A, Kerr MC, Houghton F, Lindberg A, Mitchell C, Teasdale RD, Gleeson PA. Sorting nexin 5 is localized to a subdomain of the early endosomes and is recruited to the plasma membrane following EGF stimulation. Journal of Cell Science. 2004; 117(Pt 26):6413–6424. [PubMed: 15561769]
27. Seaman MN. Endosome protein sorting: motifs and machinery. Cellular and Molecular Life Sciences. 2008; 65(18):2842–2858. [PubMed: 18726175]
28. van Weering JR, Verkade P, Cullen PJ. SNX-BAR proteins in phosphoinositide-mediated, tubular-based endosomal sorting. Seminars in Cell and Developmental Biology. 2010; 21(4):371–380. [PubMed: 19914387]
29. van Weering JR, Verkade P, Cullen PJ. SNX-BAR-Mediated Endosome Tubulation is Coordinated with Endosome Maturation. Traffic. 2012; 13(1):94–107. [PubMed: 21973056]
30. Wassmer T, Attar N, Bujny MV, Oakley J, Traer CJ, Cullen PJ. A loss-of-function screen reveals SNX5 and SNX6 as potential components of the mammalian retromer. Journal of Cell Science. 2007; 120(Pt 1):45–54. [PubMed: 17148574]
31. Carlton J, Bujny M, Peter BJ, Oorschot VM, Rutherford A, Mellor H, Klumperman J, McMahon HT, Cullen PJ. Sorting nexin-1 mediates tubular endosome-to-TGN transport through coincidence sensing of high- curvature membranes and 3-phosphoinositides. Current Biology. 2004; 14(20): 1791–1800. [PubMed: 15498486]
32. Rojas R, van Vlijmen T, Mardones GA, Prabhu Y, Rojas AL, Mohammed S, Heck AJ, Raposo G, van der Sluijs P, Bonifacino JS. Regulation of retromer recruitment to endosomes by sequential action of Rab5 and Rab7. Journal of Cell Biology. 2008; 183(3):513–526. [PubMed: 18981234]
33. Seaman MN, Harbour ME, Tattersall D, Read E, Bright N. Membrane recruitment of the cargo-selective retromer subcomplex is catalysed by the small GTPase Rab7 and inhibited by the Rab-GAP TBC1D5. Journal of Cell Science. 2009; 122(Pt 14):2371–2382. [PubMed: 19531583]
34. Henry GD, Corrigan DJ, Dineen JV, Baleja JD. Charge effects in the selection of NPF motifs by the EH domain of EHD1. Biochemistry. 2010; 49(16):3381–3392. [PubMed: 20329706]
35. Kieken F, Jovic M, Naslavsky N, Caplan S, Sorgen PL. EH domain of EHD1. Journal of Biomolecular NMR. 2007; 39(4):323–329. [PubMed: 17899392]
36. Kieken F, Sharma M, Jovic M, Giridharan SS, Naslavsky N, Caplan S, Sorgen PL. Mechanism for the selective interaction of C-terminal Eps15 homology domain proteins with specific Asn-Pro-Phe-containing partners. Journal of Biological Chemistry. 2010; 285(12):8687–8694. [PubMed: 20106972]
37. Schnatwinkel C, Christoforidis S, Lindsay MR, Uttenweiler-Joseph S, Wilm M, Parton RG, Zerial M. The Rab5 effector Rabankyrin-5 regulates and coordinates different endocytic mechanisms. PLoS Biol. 2004; 2(9):E261. [PubMed: 15328530]
38. Ito K, Ishii N, Miyashita A, Tominaga K, Kuriyama H, Maruyama H, Shirai M, Naito M, Arakawa M, Kuwano R. Molecular cloning of a novel 130-kDa cytoplasmic protein, Ankhzn, containing Ankyrin repeats hooked to a zinc finger motif. Biochemical and Biophysical Research Communications. 1999; 257(1):206–213. [PubMed: 10092534]

39. Kuriyama H, Asakawa S, Minoshima S, Maruyama H, Ishii N, Ito K, Gejyo F, Arakawa M, Shimizu N, Kuwano R. Characterization and chromosomal mapping of a novel human gene, ANKHZN. Gene. 2000; 253(2):151–160. [PubMed: 10940552]
40. Sharma M, Giridharan SS, Rahajeng J, Naslavsky N, Caplan S. MICAL-L1 links EHD1 to tubular recycling endosomes and regulates receptor recycling. Mol Biol Cell. 2009; 20(24):5181–5194. [PubMed: 19864458]
41. Heilker R, Spiess M, Crottet P. Recognition of sorting signals by clathrin adaptors. Bioessays. 1999; 21(7):558–567. [PubMed: 10472183]
42. Naslavsky N, Boehm M, Backlund PS Jr, Caplan S. Rabenosyn-5 and EHD1 interact and sequentially regulate protein recycling to the plasma membrane. Mol Biol Cell. 2004; 15(5):2410–2422. [PubMed: 15020713]
43. Cullis DN, Philip B, Baleja JD, Feig LA. Rab11-FIP2, an adaptor protein connecting cellular components involved in internalization and recycling of epidermal growth factor receptors. Journal of Biological Chemistry. 2002; 277(51):49158–49166. [PubMed: 12364336]
44. Naslavsky N, Rahajeng J, Sharma M, Jovic M, Caplan S. Interactions between EHD proteins and Rab11-FIP2: a role for EHD3 in early endosomal transport. Mol Biol Cell. 2006; 17(1):163–177. [PubMed: 16251358]
45. Rahajeng J, Panapakkam Giridharan SS, Cai B, Naslavsky N, Caplan S. MICAL-L1 is a Tubular Endosomal Membrane Hub that Connects Rab35 and Arf6 With Rab8a. Traffic. 2012; 13(1):82–93. [PubMed: 21951725]
46. Zhang J, Naslavsky N, Caplan S. Rabs and EHDs: alternate modes for traffic control. Bioscience Reports. 2012; 32(1):17–23. [PubMed: 21981138]
47. Seaman MN. Recycle your receptors with retromer. Trends in Cell Biology. 2005; 15(2):68–75. [PubMed: 15695093]
48. Belenkaya TY, Wu Y, Tang X, Zhou B, Cheng L, Sharma YV, Yan D, Selva EM, Lin X. The retromer complex influences Wnt secretion by recycling wntless from endosomes to the trans-Golgi network. Dev Cell. 2008; 14(1):120–131. [PubMed: 18160348]
49. Franch-Marro X, Wendler F, Guidato S, Griffith J, Baena-Lopez A, Itasaki N, Maurice MM, Vincent JP. Wingless secretion requires endosome-to-Golgi retrieval of Wntless/Evi/Sprinter by the retromer complex. Nat Cell Biol. 2008; 10(2):170–177. [PubMed: 18193037]
50. Harterink M, Port F, Lorenowicz MJ, McGough IJ, Silhankova M, Betist MC, van Weering JR, van Heesbeen RG, Middelkoop TC, Basler K, Cullen PJ, Korswagen HC. A SNX3-dependent retromer pathway mediates retrograde transport of the Wnt sorting receptor Wntless and is required for Wnt secretion. Nat Cell Biol. 2011; 13(8):914–923. [PubMed: 21725319]
51. Pan CL, Baum PD, Gu M, Jorgensen EM, Clark SG, Garriga G. C. elegans AP-2 and retromer control Wnt signaling by regulating mig-14/Wntless. Dev Cell. 2008; 14(1):132–139. [PubMed: 18160346]
52. Port F, Kuster M, Herr P, Furger E, Banziger C, Hausmann G, Basler K. Wingless secretion promotes and requires retromer-dependent cycling of Wntless. Nat Cell Biol. 2008; 10(2):178–185. [PubMed: 18193032]
53. Yang PT, Lorenowicz MJ, Silhankova M, Coudreuse DY, Betist MC, Korswagen HC. Wnt signaling requires retromer-dependent recycling of MIG-14/Wntless in Wnt-producing cells. Dev Cell. 2008; 14(1):140–147. [PubMed: 18160347]
54. Ang AL, Taguchi T, Francis S, Folsch H, Murrells LJ, Pypaert M, Warren G, Mellman I. Recycling endosomes can serve as intermediates during transport from the Golgi to the plasma membrane of MDCK cells. J Cell Biol. 2004; 167(3):531–543. [PubMed: 15534004]
55. Caplan S, Hartnell LM, Aguilar RC, Naslavsky N, Bonifacino JS. Human Vam6p promotes lysosome clustering and fusion in vivo. J Cell Biol. 2001; 154(1):109–122. [PubMed: 11448994]
56. Presley JF, Cole NB, Schroer TA, Hirschberg K, Zaal KJ, Lippincott-Schwartz J. ER-to-Golgi transport visualized in living cells. Nature. 1997; 389(6646):81–85. [PubMed: 9288971]
57. Ying M, Grimmer S, Iversen TG, Van Deurs B, Sandvig K. Cholesterol loading induces a block in the exit of VSVG from the TGN. Traffic. 2003; 4(11):772–784. [PubMed: 14617359]

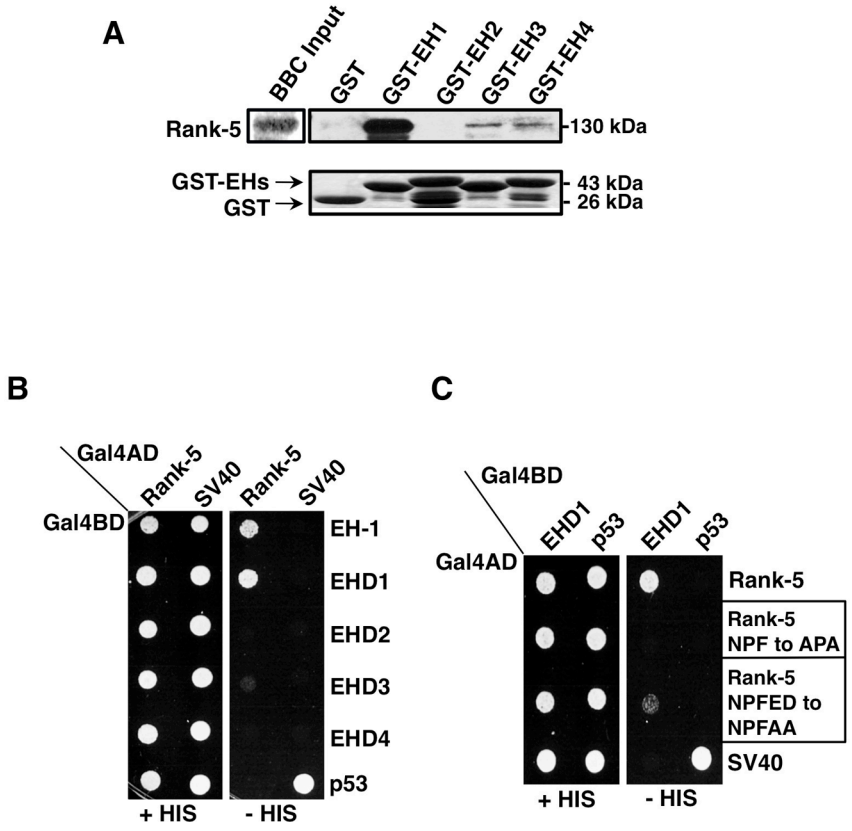

Figure 1. Rank-5 interacts with EHD1 via its NPF-motif

(A) GST-EH-domains of EHD1-4 were used to pull-down Rank-5 from bovine brain cytosol (BBC). Upper panel shows the Western Blot results; lower panel shows the equal loading of GST-fusion proteins by Coomassie Blue staining. (B) Yeast two-hybrid interactions between WT Rank-5 and the EH-domain of EHD1 (EH-1), and full-length EHD1-4. The *S.cerevisiae* yeast strain AH109 was co-transformed with the indicated Gal4-binding domain (Gal4BD) fusion constructs and Gal4-activation domain (Gal4AD)-SV40 (control), together with the indicated Gal4AD fusion constructs with Gal4BD-p53 (control). Co-transformants were plated on non-selective (+HIS) and selective (−HIS) media. (C) Yeast two-hybrid interaction between Rank-5 NPF-motif mutations and EHD1.

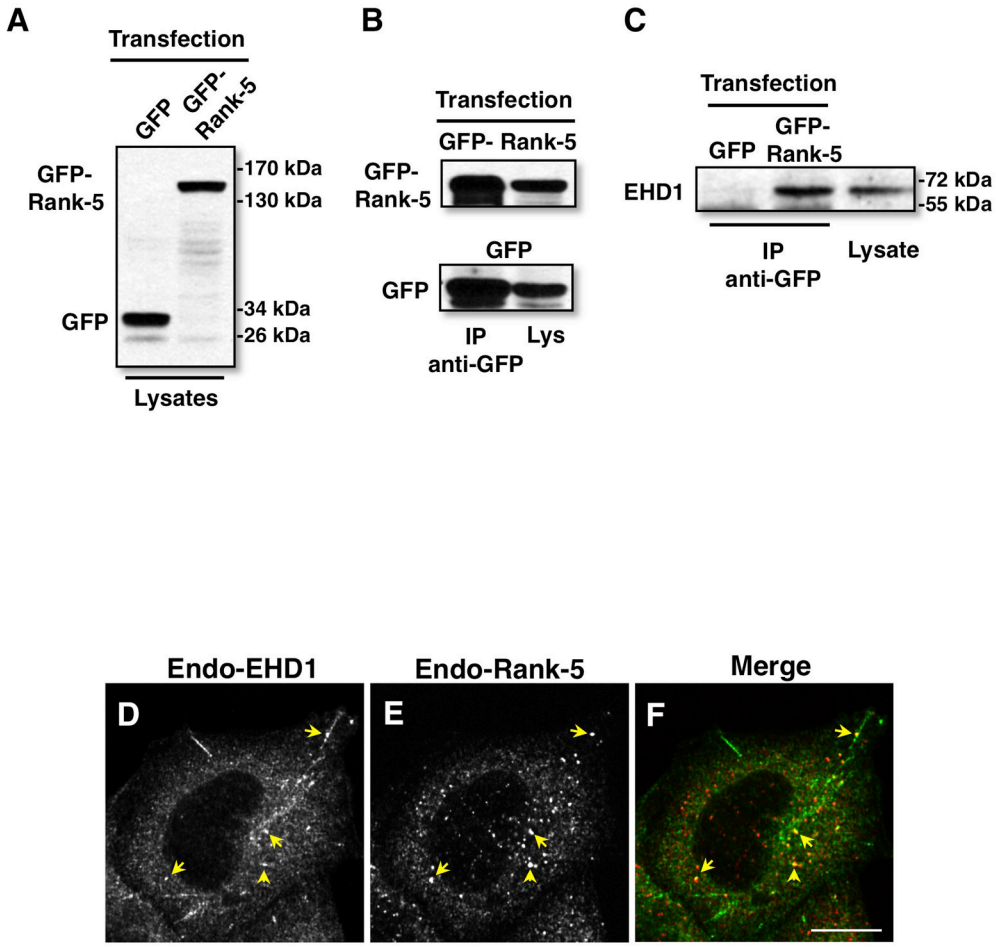

Figure 2. Rank-5 associates with EHD1 *in vivo*

(A–C) Co-immunoprecipitation of Rank-5 and EHD1. HeLa cells were transfected with GFP-Rank-5 or GFP, and transfection efficiency was verified by immunoblot (A). After 48 h, cells were lysed and subjected to immuniprecipitation and detection with anti-GFP antibody (B), or were immunoblotted with anti-EHD1 antibody (C). (D–F) Partial co-localization between Rank-5 and EHD1. HeLa cells were stained with rabbit anti-EHD1 (D) and mouse anti-Rank-5 (E) antibodies. Arrows depict representative structures containing both endogenous proteins. Bar, 10 μm.

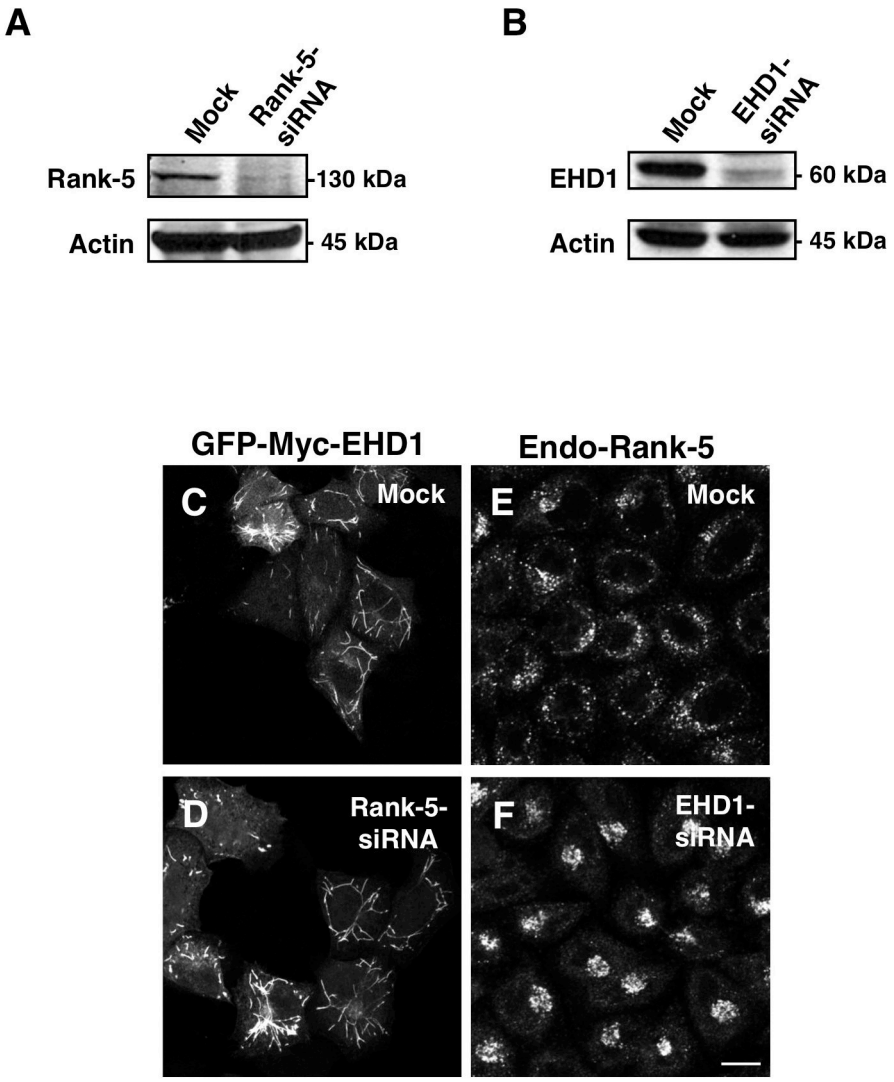

Figure 3. EHD1 regulates localization of Rank-5

(A, B) Knock-down of Rank-5 and EHD1 by siRNA. HeLa cells were either mock-treated or treated with Rank-5-siRNA (A) or EHD1-siRNA (B) for 48 h. Total cell lysates were subjected to SDS-PAGE and immunoblotted with the indicated antibodies. (C, D) Effect of Rank-5 depletion on EHD1 localization. HeLa cells were either mock-treated (C) or treated with Rank-5-siRNA (D), and transiently transfected with GFP-Myc-EHD1. (E, F) Effect of EHD1 depletion on Rank-5 localization. HeLa cells were either mock-treated (E) or treated with EHD1-siRNA (F), and stained with mouse anti-Rank-5 antibody. Bar, 10 μm.

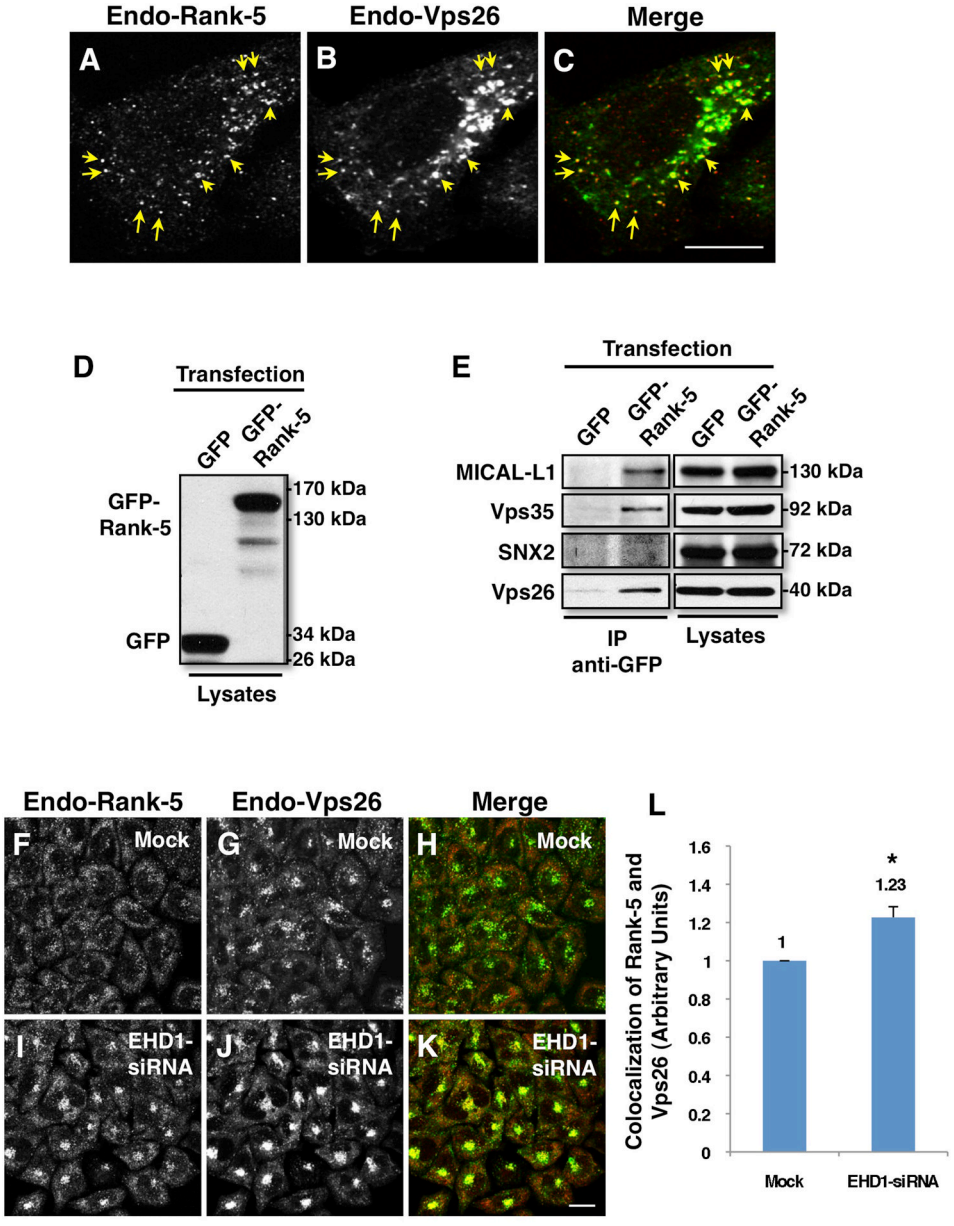

Figure 4. Rank-5 associates with Vps26 and Vps 35 *in vivo*

(A–C) Partial co-localization between Rank-5 and the retromer component Vps26. HeLa cells were stained with mouse anti-Rank-5 (A) and rabbit anti-Vps26 (B) antibodies. Arrows depict representative structures containing both endogenous proteins. (D, E) HeLa cells were transfected with GFP-Rank-5 or GFP for 48 h (D). Cells were then lysed and subjected to immunoprecipitation with anti-GFP antibody. Immunoprecipitates were resolved by SDS-PAGE and immunoblotted with anti-MICAL-L1, anti-Vps35, anti-SNX2 or anti-Vps26 antibody (E). (F–L) Effect of EHD1 depletion on the co-localization of Rank-5 and Vps26. HeLa cells were either mock-treated (F, G, H) or treated with EHD1-siRNA (I, J, K), and stained with mouse anti-Rank-5 (F, I) and rabbit anti-Vps26 (G, J) antibodies. Co-localization was quantified by ImageJ (L). Values are represented as means ± s.e.m. of three experiments. $*P < 0.05$, Student's *t*-test. Bar, 10 μm.

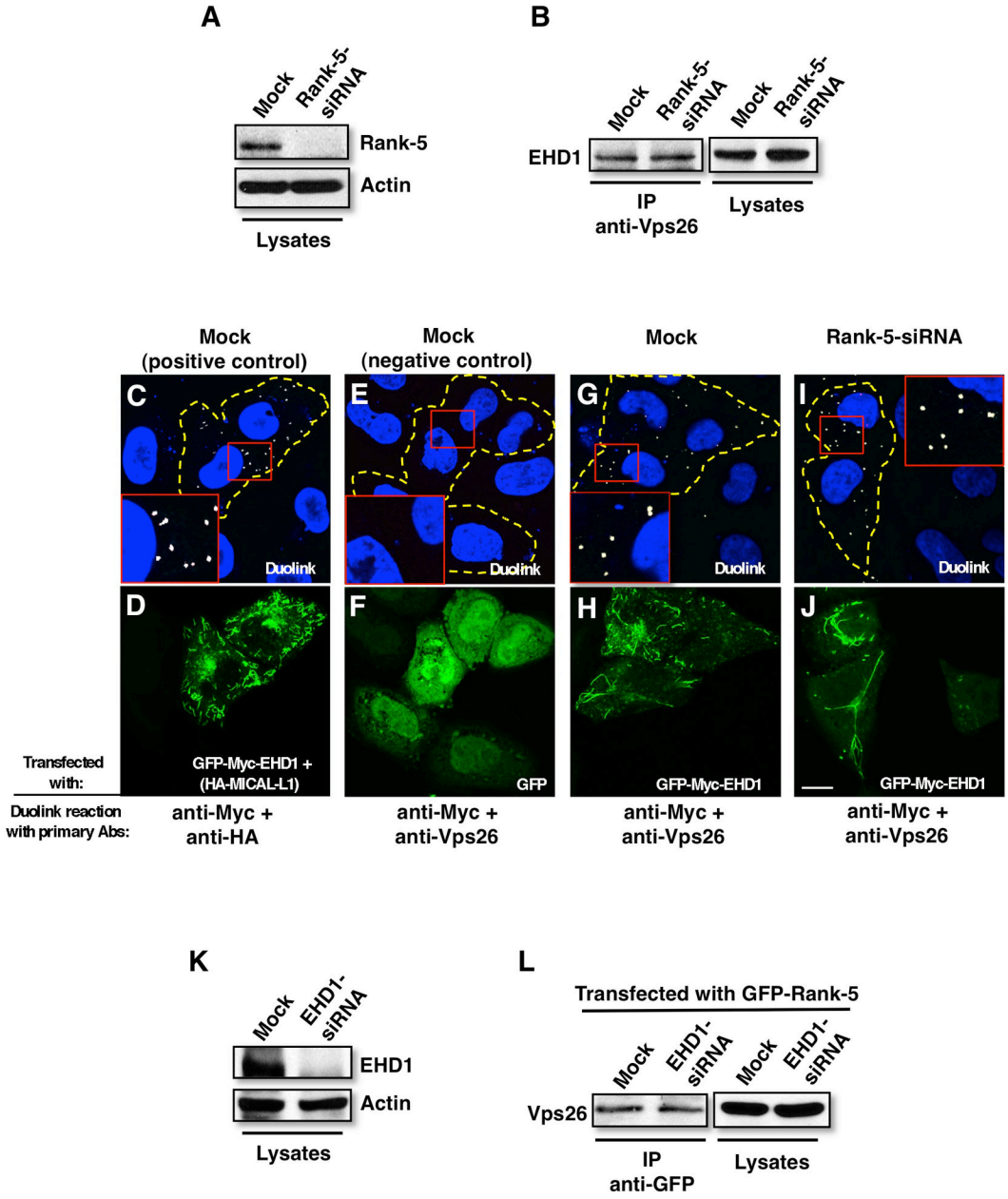

Figure 5. The association between EHD1, Rank-5 and Vps26

(A, B) Effect of Rank-5 depletion on the co-immunoprecipitation of EHD1 and Vps26. HeLa cells were either mock-treated or treated with Rank-5-siRNA (A), and cell lysates were immunoprecipitated with anti-Vps26 antibody. Immunoprecipitates were resolved by SDS-PAGE and immunoblotted with anti-EHD1 antibody (B). (C–J) Duolink analysis of Rank-5 depletion on the association between EHD1 and Vps26. HeLa cells grown on coverslips were either mock-treated (G, H) or treated with Rank-5-siRNA (I, J), and transiently transfected with GFP-Myc-EHD1. Cells were then incubated with mouse anti-Myc and rabbit anti-Vps26 antibodies (G–J) and the Duolink analysis was performed according to manufacturer's protocol. Positive association of proteins is reflected by white dots. A positive control was performed by co-transfecting with GFP-Myc-EHD1 and HA-MICAL-L1 in mock-treated cells, incubated with anti-Myc and anti-HA antibodies (C, D).

A negative control was performed by transfecting GFP in mock-treated cells incubated with anti-Myc and anti-Vps26 antibodies (E, F). Dashed borders depict GFP or GFP-Myc-EHD1 transfected cells. Boxed areas are magnified and depicted in the insets. Bar, 10 μm. (K, L) Effect of EHD1 depletion on the co-immunoprecipitation of Rank-5 and Vps26. HeLa cells were either mock-treated or treated with EHD1-siRNA (K), and transfected with GFP-Rank-5. Cell lysates were immunoprecipitated with anti-GFP antibody. Immunoprecipitates were resolved by SDS-PAGE and immunoblotted with anti-Vps26 antibody (L).

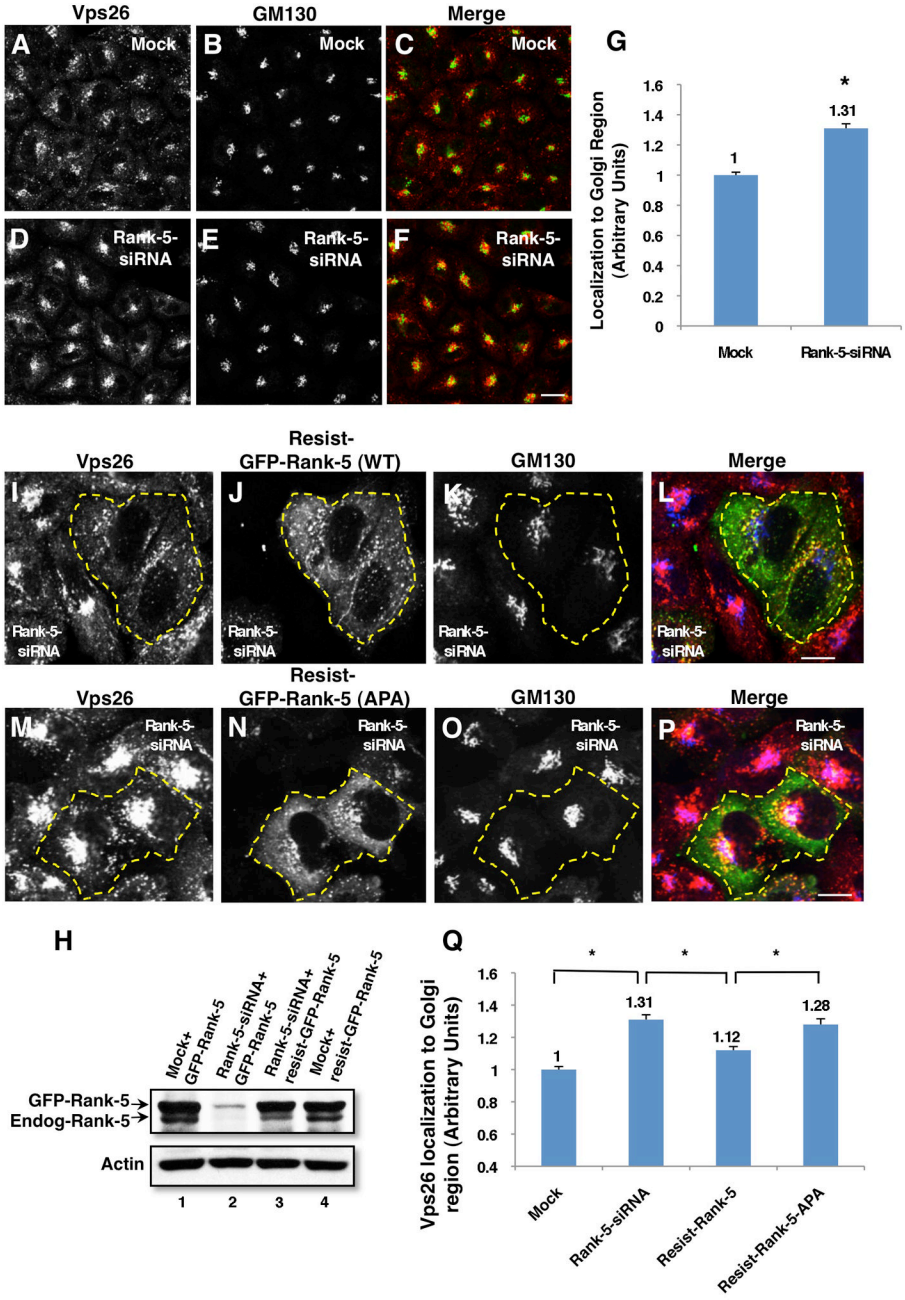

Figure 6. Depletion of Rank-5 affects the localization of the retromer Vps26 subunit

(A–G) Effect of Rank-5 knock-down on the localization of Vps26. HeLa cells grown on coverslips were either mock-treated (A–C) or treated with Rank-5-siRNA (D–F), and co-stained with rabbit anti-Vps26 and mouse anti-GM130. Co-localization was quantified by ImageJ (G). (H–Q) Rescue of Vps26 localization by re-introduction of Rank-5 but not the Rank-5 NPF to APA mutant. (H) Western blot demonstrating Rank-5 knock-down following Rank-5-siRNA and rescue of Rank-5 expression by siRNA-resistant Rank-5 constructs. HeLa cells were mock-treated and transfected with either wildtype (WT) GFP-Rank-5 (lane 1) or siRNA-resistant GFP-Rank-5 (lane 4). In parallel, cells were treated with Rank-5-siRNA and transfected with either WT GFP-Rank-5 (lane 2) or siRNA-resistant GFP-Rank-5 (siRNA + Rescue, lane 3) for 48 h. Total cell lysates were subjected to SDS-PAGE

and immunoblotted with anti-Rank-5 and anti-actin antibodies. (I–P) Rescue of Vps26 distribution by WT or APA siRNA-resistant GFP-Rank-5. Cells were treated with Rank-5-siRNA and transfected with WT siRNA-resistant GFP-Rank-5 (J) or with APA mutant (N), and stained with anti-Vps26 (I, M) and anti-GM130 (K, O). The merged images are depicted in L and P. Dashed borders depict WT or APA siRNA-resistant GFP-Rank-5 transfected cells. Co-localization of Vps26 to the Golgi was quantified by ImageJ (Q). Values are represented as means ± s.e.m. of three experiments. $*P < 0.05$, Student's *t*-test. Bar, 10 μm.

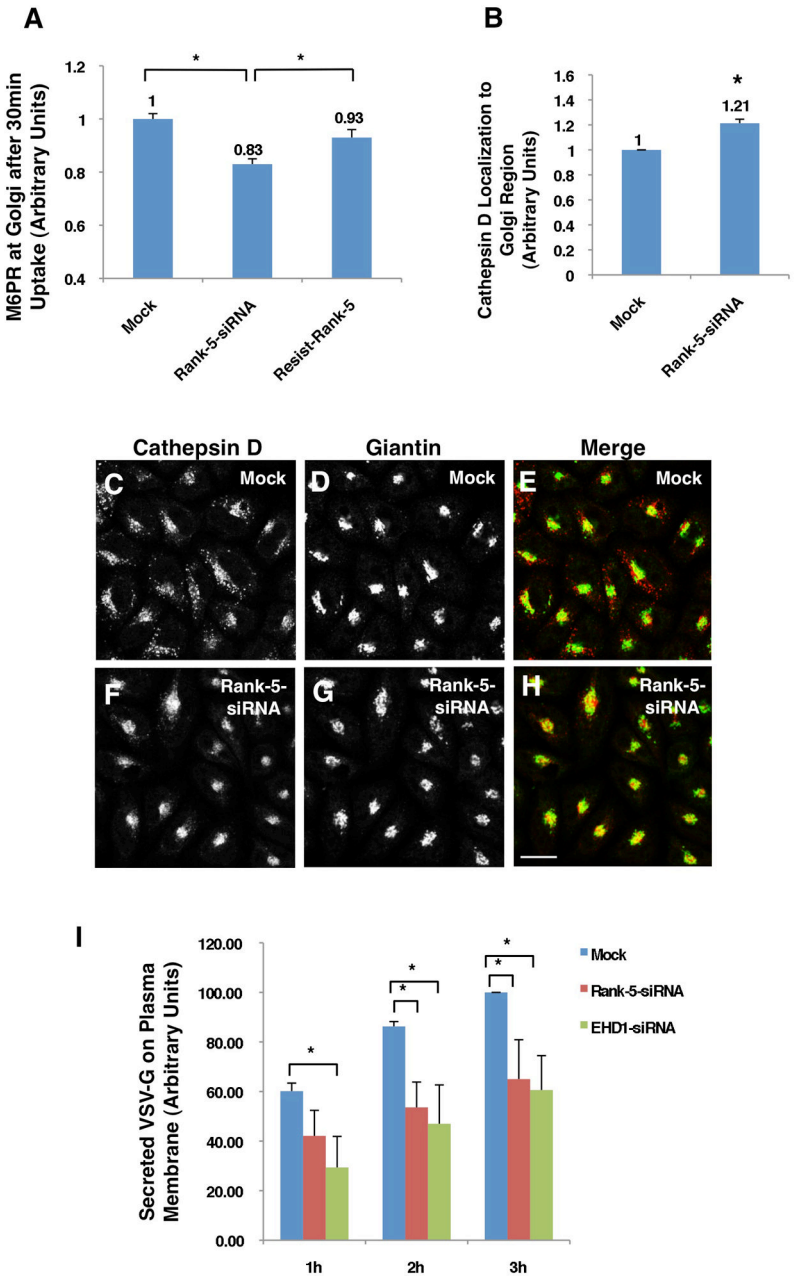

Figure 7. Rank-5 depletion impairs M6PR retrieval from endosomes, biosynthetic transport of cathepsin D, and secretion of VSV-G

(A) Effect of Rank-5 knockdown on the retrieval of M6PR. HeLa cells grown on coverslips were Mock-treated or treated with Rank-5-siRNA, and transfected with WT siRNA-resistant GFP-Rank-5. Cells were subjected to anti-M6PR antibody uptake assay for 30 min followed by antibody staining and quantification (n=150). (B–H) Effect of Rank-5 knockdown on the localization of cathepsin D to the Golgi. HeLa cells were either mock-treated (C–E) or treated with Rank-5-siRNA (F–H), and co-stained with anti-cathepsin D and anti-Giantin. Quantification of the localization of cathepsin D to the Golgi was assessed with Image J software (B). (I) Flow cytometry analysis of VSV-G secretion to the plasma membrane upon knockdown of Rank-5 or EHD1. HeLa cells plated in 35 mm dishes were either mock-treated or treated with Rank-5-siRNA or EHD1-siRNA, and transfected with GFP-VSV-G.

Cells were transferred to 40°C for 18 h, and shifted to 32°C for various time points. Secreted VSV-G to the plasma membrane was detected by anti-VSV-G followed by a Cy5-conjugated secondary antibody and subjected to flow cytometry analysis. Values are represented as means ± s.e.m. of three experiments. $*P < 0.05$, Student's *t*-test. Bar, 10 μm.

Table 1

Thermodynamic parameters for the interaction of wild type and mutant peptide with protein determined by ITC at 25 °C.

Peptide	ΔH_b (kcal/mol)	n	$K_b \times 10^{-3}$ (M^{-1})	$\Delta G_b°$ (kcal/mol)	$T\Delta S$ (kcal/mol)
Wild Type	−3.6	1.0	23	−6.0	2.4
Mutant	−4.0	1.0	2.8	−4.7	0.7

All experiments are done in buffer containing 100 mM KCl, 20 mM Tris and 2 mM CaCl2 at pH 7.0. Experimental errors are as follows: ΔH_b (± 5 %), ΔK_b (± 20 %), $T\Delta S$ (± 5 %) and $\Delta G°_{(20)}$(± 7%).